

Insights into the Mechanism and Regioselectivity of Palladium-Catalyzed Arylation of α,β -Unsaturated Ketones

Jinbo Luo, Xiaoxi Su, Zhizheng Chen, Shuanglin Qu*

College of Chemistry and Chemical Engineering, State Key Laboratory of Chemo/Biosensing and Chemometrics, Hunan University, Changsha 410082, P. R. China.

Keywords: DFT; Palladium; Arylation; Proton shuttle.

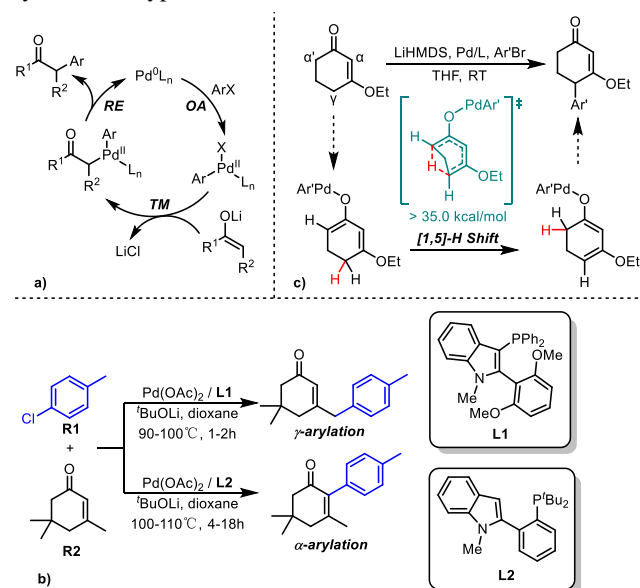
ABSTRACT: Transition-metal catalyzed coupling reactions of carbonyl compounds using simple chemical feedstocks have become a cornerstone of modern synthetic organic chemistry. The mechanisms and origins for ligand-controlled palladium-catalyzed regioselective α - and γ -arylation of α,β -unsaturated ketones with aryl halides have been investigated by density functional theory (DFT) calculations. Computational results have confirmed our proposed catalytic cycle, which includes four steps: oxidative addition, transmetalation, deprotonation/protonation, and reductive elimination. The Heck-type mechanism for α -arylation of α,β -unsaturated ketones is proved to be less feasible due to the high energy barrier for the insertion step. While reductive elimination is the rate-determining step (RDS), the critical process responsible for the regioselectivity depends upon the direction of protonation step, where the base function as a proton shuttle to facilitate H migration. Distortion/interaction analysis, natural bond orbital (NBO) analysis, and buried volume calculations indicate that the regioselectivity is primarily controlled by the steric hindrance at the region of the ligand close to the enone. The indole ring of the phosphine ligand lay upward or downward, varying the space crowding in the region, thus leading to different protonation products followed by corresponding reductive elimination. The phenomenon of [1,5]-H transfer discovered in the γ -arylation of β -alkoxy cyclohexenones is also well rationalized by the proton shuttle model.

INTRODUCTION

The functionalization of C–H bonds plays a pivotal role in organic synthesis due to its wide application in synthesizing complex compounds such as pharmaceuticals and natural products.^{1–3} Palladium-catalyzed arylation of carbonyl compounds has been dramatically developed in the past two decades, as it provides a convenient method for constructing C–C bonds.^{4–6} In 1997, the first Pd-catalyzed direct α -arylation of ketones with aryl halides was almost simultaneously reported by Buchwald and Hartwig,^{7,8} who established a milestone in this field of research. Since then, more and more coupling reactions between aryl halides or pseudohalides⁹ and carbonyl compounds including ketones, aldehydes, esters, amides, lactones,¹⁰ lactams¹¹ and cyclic ketones by the catalysis of palladium have been discovered,⁴ and the applications of these reactions in the synthesis were gradually developed.¹² While many studies reported on the α -arylation of carbonyl compounds, research focusing on the γ -arylation was gradually increasing. Up to now, there are plenty of reports about the Pd-catalyzed γ -arylation of α,β -unsaturated carbonyl compounds such as α,β -unsaturated ketone,^{13–16} aldehydes,¹⁷ lactones¹⁸ and even α,β -unsaturated nitriles¹⁹ because of its strongly electron-withdrawing ability.²⁰

The mechanism of Pd-catalyzed α -arylation of carbonyl compounds is generally believed to include the following processes: (i) oxidative addition of aryl halides (ArX, X = Cl, Br or I) to the Pd(0)L_n (n = 1 or 2); (ii) transmetalation between [Pd(II)L_n(Ar)(X)] complex and Li, Na, or K-enolates generated by the reaction of the carbonyl compounds with strong bases like *t*-BuOLi, *t*-BuONa, and LiHMDS *et al.*; (iii) reduc-

tive elimination occurs to form coupling products and regenerate Pd(0)L_n (Scheme 1a). Similarly, the γ -arylation reaction mechanism also mainly includes the steps of oxidative addition, transmetalation, and reductive elimination. However, as there is a carbon-carbon double bond in α,β -unsaturated carbonyl compounds, their α -arylation product can be generated by the Heck-type reaction mechanism.^{5, 15, 21}



Scheme 1. (a) General mechanism of Pd-catalyzed α -arylation of carbonyl compounds. (b) Ligand-controlled Pd-catalyzed regioselective arylation of α,β -unsaturated

ketones. (c) Pd-catalyzed γ -arylation of β -alkoxy cyclohexenones.

Franzoni's DFT study on Pd-catalyzed γ -arylation of α,β -unsaturated aldehyde found that the palladium atom undergoes smooth transitions from η^1 to η^3 coordination modes with the enone moiety, leading to up to ten palladium enolates that serve as precursors for the subsequent reductive elimination and rationalized the γ -selectivity observed.²² By comparing several modes of reductive elimination, Orlandi disclosed that the factors controlling the enantioselectivity of Pd-catalyzed α -arylation of ketones were the electrostatic interaction and the steric repulsion in the reductive elimination step.²³

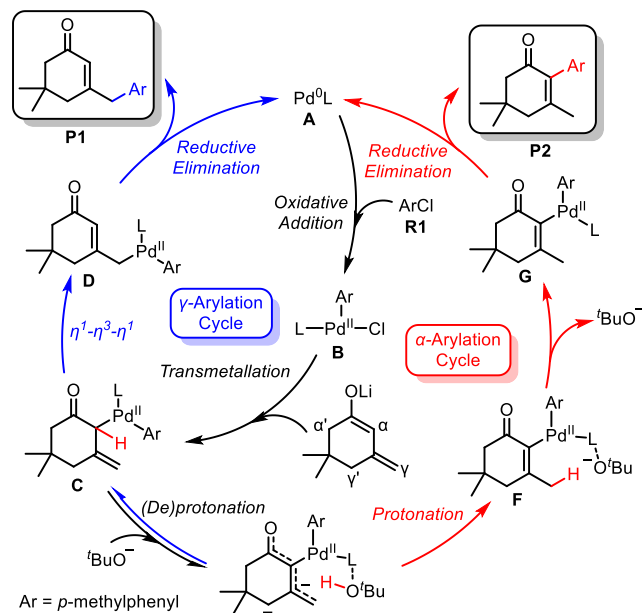
Recently, On Ying Yuen reported the first ligand control of Pd-catalyzed site-selective α - and γ -arylation of α,β -unsaturated ketones with aryl halides (Scheme 1b), and Li-Dong Shao reported the Pd-catalyzed γ -arylation of β -alkoxy cyclohexenones (Scheme 1c).^{24, 25} Through experimental mechanism investigations, they all observed that there was an H shift phenomenon during their reaction, and Shao proposed that it was mainly determined by the tunneling effect. Since α,β -unsaturated ketone (enone) fragments have multiple reaction sites and exist in many biologically active substances,^{26, 27} the reactions discovered by Yuen and Shao have important theoretical and practical significance.

Although the experimenters proposed their hypothesis for the mechanism of the reaction, a sound explanation for the origins of the selectivity and the details of the H shift remains to be disclosed. Because of these issues, we decided to carry out a detailed mechanistic study on the reaction reported by Yuen with the aid of DFT calculations. By calculating the structures/energetics associated with relevant reaction intermediates and transition states, we expect to explain why different ligands can determine the regioselectivity observed in the experiments and reveal the details of the H migration phenomenon. We hope that this study would provide insights related to catalysis involving the palladium metal.

COMPUTATIONAL DETAILS

All calculations were performed by using the Gaussian 16 package.²⁸ All geometries were optimized in the gas phase at B3LYP-D3(BJ)²⁹⁻³²/BSI level, where BSI represents a basis set SDD^{33, 34} was used to describe Pd atom, and 6-31G(d, p)^{35, 36} for H, Li, C, N, O, Cl and P atoms. Frequency calculations were performed at the same level theory for all optimized structures to ensure that every optimized structure has no imaginary frequency and that all optimized transition states have only one imaginary frequency. Intrinsic Reaction Coordinate (IRC)³⁷ calculations were carried out to make sure that each transition state links two relevant intermediates. Finer single-point energy calculations were performed at M06³⁸/BSII level, including solvation effects with the SMD³⁹ continuum solvation model for 1,4-dioxane. The basis set BSII is a combination of SDD for Pd and 6-311++G(d, p)⁴⁰⁻⁴² for all other atoms. All frequencies below 50 cm⁻¹ were replaced by 50 cm⁻¹ when computing vibrational entropies.⁴³ Partial atomic charges were calculated at the M06/BSII level using the Natural Population Analysis (NPA) method which relies on localized Natural Bond Orbitals (NBOs).⁴⁴⁻⁴⁶ The three-dimensional (3D) structures were visualized with the aid of CYLview20 software.⁴⁷

RESULTS AND DISCUSSION



Scheme 2. Possible catalytic cycle for Pd-catalyzed regioselective arylation of α,β -unsaturated ketones.

Based on previous studies, we proposed a catalytic cycle for the α - and γ -arylation of α,β -unsaturated ketones (Scheme 2).²²⁻²⁴ Due to the widespread synthetic utility of α,β -unsaturated cyclic ketones fragment,⁴⁸ the *p*-chlorotoluene and isophorone experimentally employed were chosen as the model substrates in this theoretical calculation. Palladium acetate was first reduced by the phosphine ligand to zero-valent palladium complex **A**,⁴⁹⁻⁵¹ which was believed to be the catalytically active species in this catalytic system. Oxidative addition of aryl chloride to Pd(0) species provides the complex **B**, and then **B** undergoes transmetalation with lithium enolate that is generated *in situ* with lithium tert-butoxide to generate intermediate **C**. The excessive base in the reaction system can abstract the active C(α)-H, so the complex **E** becomes the cross-point of the α - and γ -arylation cycle. Both C(α) and C(γ)-protonation by tert-butanol are possible, producing **C** and **F** respectively. While complex **C** undergoes a η^1 - η^3 - η^1 transformation forms **D** species followed by the reductive elimination to produce γ -arylated product, $t\text{-BuO}^-$ leaves to form **G** and finally generate α -arylated product.

Due to both **L1** and **L2** being bulky ligands, the monoligated palladium complex PdL rather than PdL₂ was taken as the reference point for energy consideration in this theoretical calculation (Figure 1).^{21, 52, 53} Starting from the catalytically active species **CAT1**, one molecule of ArCl first coordinates with Pd(0)L¹, and then undergoes a classic three-membered cyclic transition state **TS1** to generate the oxidative addition product *cis*-**INT2** with an activation free energy of 11.3 kcal/mol, which can rapidly occur under the reported reaction condition. The *cis*-[Pd(II)L¹(Ar)(Cl)] is easy to isomerize into the *trans*-[Pd(II)L¹(Ar)(Cl)] (that is, Cl is at the *para* position of Ar), and the mechanism of this process has been studied thoroughly.⁵⁴⁻⁵⁷ However, the Gibbs free energy of *trans*-**INT2** is 6.1 kcal/mol higher than that of *cis*-**INT2** in our calculations, which is quite different from previous reports that *trans* adducts are usually more stable than *cis*.⁵⁸⁻⁶⁰ The Pd-Cl bond in the *cis*-**INT2** (2.35 Å) is shorter than the *trans*-**INT2**

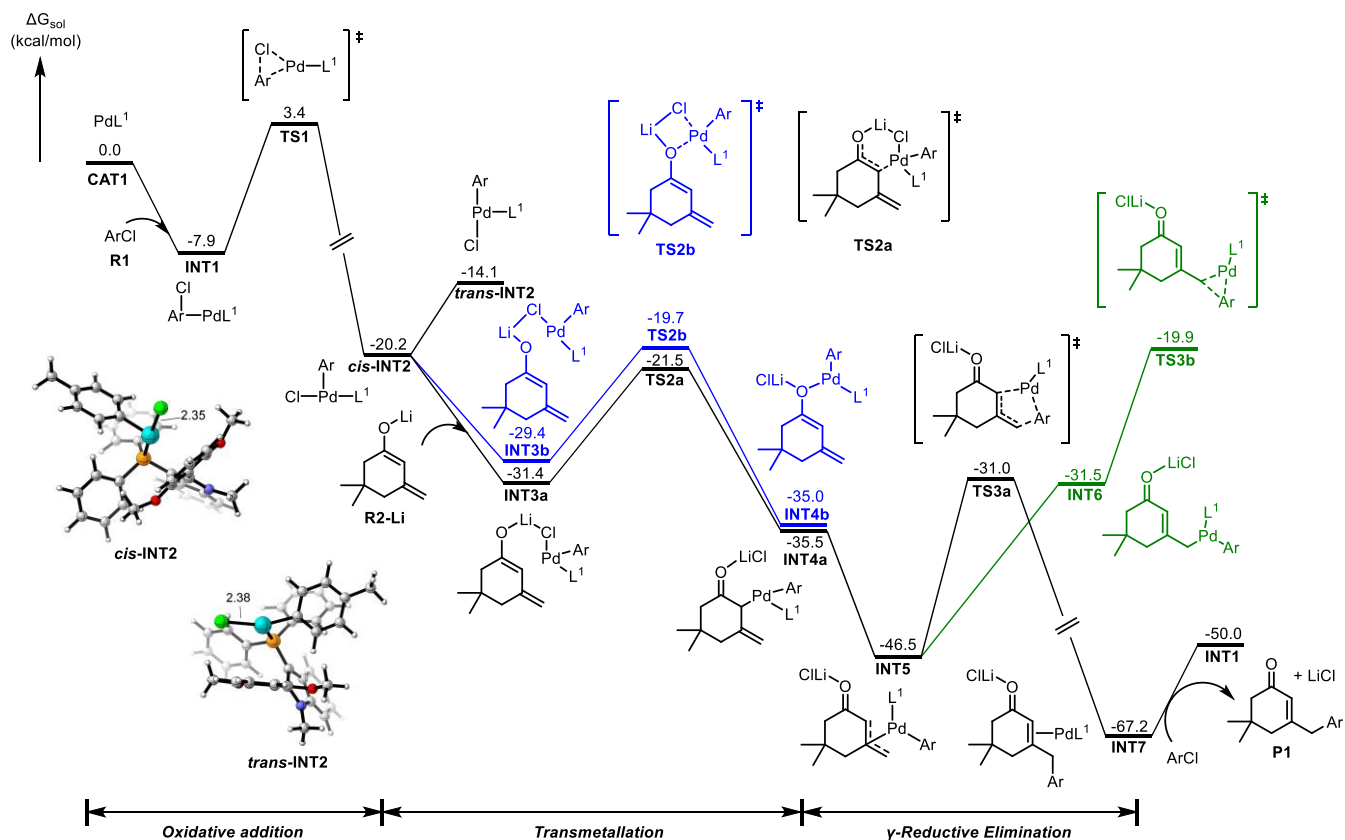


Figure 1. Energy profile for γ -arylation of isophorone catalyzed by PdL^1 .

(2.38 Å), which may be attributed to the weak *trans* effect between the phosphine ligand and chlorine ligand.^{58, 61} In the *trans* structure, the steric repulsion between the ligand and the aryl group may also lead to an increase in energy as the aryl group is close to the phosphine ligand.

Since the *cis*- $[\text{Pd}(\text{II})\text{L}^1(\text{Ar})(\text{Cl})]$ is more stable than *trans*- $[\text{Pd}(\text{II})\text{L}^1(\text{Ar})(\text{Cl})]$, we will only discuss *cis*- $[\text{Pd}(\text{II})\text{L}^1(\text{Ar})(\text{Cl})]$ in the next transmetalation step and the *trans*- $[\text{Pd}(\text{II})\text{L}^1(\text{Ar})(\text{Cl})]$ is discussed in Figure S2. While the experimenter believes that isophorone forms an organolithium compound with *t*-BuOLi, our calculations show that the intermediate of the organolithium compound is unstable and will easily transform into a lithium enolate intermediate **R2-Li** (Figure S1). There are two mechanisms of the transmetalation step between Li-enolate and *cis*- $[\text{Pd}(\text{II})\text{L}^1(\text{Ar})(\text{Cl})]$, one is classical four-membered ring transmetalation to provide the O-bound Pd-enolate, and the other is six-membered ring transmetalation to obtain the C-bound Pd-enolate.²³ Both **INT3a** and **TS2a** have lower free energy than **INT3b** and **TS2b**, which is 2.0 kcal/mol and 1.8 kcal/mol respectively. Although the free energies of the transmetalation products **INT4a** and **INT4b** are almost the same, comparing the two transition states, it is more inclined to the six-membered ring enolate palladium process in the transmetalation.

Lewis acids (LA) have been found to activate carbonyl compounds in many studies and can stabilize the transition state by the interaction between LA and the carbonyl oxygen atom,⁶²⁻⁶⁴ and we also found such a situation in the process of reductive elimination. Without LiCl, the reaction energy barrier of the reductive elimination step is as high as 25.2 kcal/mol (Figure S3), so in the following, only the reductive elimination

step with the transmetalation product LiCl bound to the carbonyl oxygen atom is discussed. In **INT4a**, the Li atom of the LiCl is bound to the carbonyl oxygen atom, while Pd coordinates with C(α) in η^1 manner. However, Pd atoms can either form **INT6** in the η^1 coordination mode with C(γ) through a fast η^1 - η^3 - η^1 isomerization or form **INT5** in the η^3 coordination mode.²² Therefore, there will be two different modes in the reductive elimination step: three-membered ring reductive elimination and five-membered ring reductive elimination.

Whether five-membered or three-membered ring reductive elimination, a transformation from η^1 -Pd enolate to η^3 -Pd enolate is required to obtain the corresponding product. The isomerization from **INT4a** to **INT5** is exergonic by 11.0 kcal/mol, and the following **INT5** isomerize to **INT6** is endergonic by 15.0 kcal/mol, which means the η^3 -Pd enolate is the stabler intermediate. The reductive elimination energy barrier of the three-membered ring is 11.1 kcal/mol higher than that of the five-membered ring (**TS3b** vs. **TS3a**), thus the reductive elimination mode of the five-membered ring is more favorable. Finally, the γ -arylated α,β -unsaturated ketone molecule in **INT7** was replaced by a molecule of *p*-chlorotoluene to form **INT1** to enter the next catalytic cycle. During the γ -arylation cycle, the energy barrier of the reductive elimination step is 15.5 kcal/mol (**TS3a**-**INT5**), which is the rate-determining step in the entire catalytic cycle.

For α -arylation of isophorone catalyzed by PdL^2 , there are two reaction mechanisms, one is the palladium enolate mechanism similar to the γ -arylation cycle catalyzed by PdL^1 , and the other is a Heck-type reaction mechanism.^{15, 65, 66} Considering that the experimental observation that [1,3]-H transfer

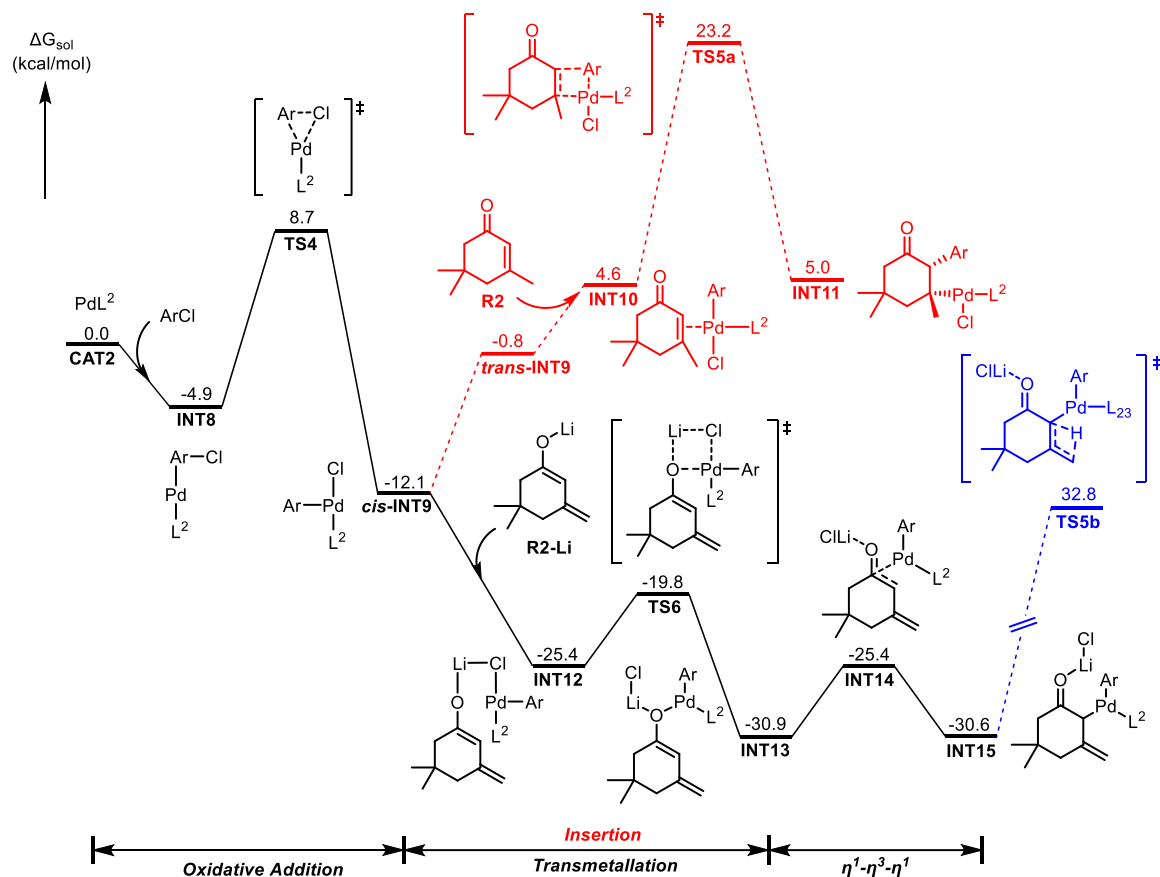


Figure 2. Heck-type mechanism (in red) and palladium enolate mechanism (in black) for the PdL^2 -catalyzed α -arylation of isophorone.

occurred during their mechanistic research in α -arylation process, we think it is necessary to reveal what type of mechanism it is and the detailed mechanism of [1,3]-H migration process. The total catalytic cycle proposed for the Heck-type mechanism is shown in Figure S4.

As is shown in Figure 2, both the Heck-type mechanism and the palladium enolate mechanism first undergo oxidative addition of aryl chloride to $\text{Pd}(0)$ species **CAT2** to obtain *cis*-**INT9** with an activation energy barrier of 13.6 kcal/mol (**TS4**–**INT8**), which is not much different from the **CAT1** (11.3 kcal/mol). For the Heck-type mechanism, *cis*-**INT9** must isomerize into *trans*-**INT9** to free up the coordination site to facilitate the insertion of the carbon-carbon double bond of isophorone into the $\text{Pd-C}(sp^2)$ bond. In the next step of carbon-carbon double bond insertion into $\text{Pd-C}(sp^2)$ bond, the activation energy barrier is as high as 35.3 kcal/mol (**TS5a**–*cis*-**INT9**), which means that the Heck-type α -arylation mechanism is infeasible.

Both *cis*-**INT9** and *trans*-**INT9** can undergo transmetalation with lithium enolate **R2-Li**, but for brevity, we only draw the most favorable transmetalation mode in Figure 2, and the rest are shown in Figure S5. In the PdL^2 -catalyzed α -arylation of isophorone, the O-bound Pd-enolate **INT13** is generated by *cis*-**INT9** and **R2-Li** through a four-membered ring transmetalation transition state (**TS6**) with an activation free energy of 5.6 kcal/mol. Due to σ -bonded groups in transition-metal complexes can rearrange to π -bonded ligands and vice versa,^{22, 67, 68} the palladium enolate intermediate **INT13** can easily isomerize into **INT14** and **INT15** which is similar to the η^1 - η^3 - η^1 isomerization in γ -arylation cycle.

As the reductive elimination of **INT15** forms $\text{C}(sp^3)$ – $\text{C}(sp^2)$ bond instead of $\text{C}(sp^2)$ – $\text{C}(sp^2)$ bond between the aryl and enone moiety, the [1,3]-H transfer observed in the reaction is necessary to obtain the α -arylated product. The energy barrier for the H atom at the α -position of **INT13** to migrate directly to $\text{C}(\gamma)$ via **TS5b** is more than 60 kcal/mol (**TS5b**–**INT15**), which indicates that the direct H shift path is impossible under the experimental conditions. Considering the presence of excessive *t*-BuOLi in the reaction system, we speculate that tert-butoxide may act as a proton shuttle to assist H migration (Figure 3a).^{69–71}

In **INT15**, there is a $\text{C}(\alpha)$ –H which is located at the α position of the carbonyl group and the allyl position at the same time, so it is a relatively strong acidic H and is easy to be taken away by the excess base in the reaction system. The tert-butoxide first coordinates with the palladium center, and this process is exergonic by 8.7 kcal/mol. Then, through the transition state **TS7**, the H on $\text{C}(\alpha)$ is abstracted and transferred to the oxygen atom with an activation free energy of 13.4 kcal/mol (**TS7**–**INT16**). After the H is taken away by *t*-BuO[−], the entire enone fragment in **INT17** is negatively charged. The natural population analysis shows that the charge on $\text{C}(\alpha)$ and $\text{C}(\gamma)$ is -0.368 and -0.598 respectively, so it is easy for $\text{C}(\gamma)$ to take back the H in the *t*-BuOH through **TS8** with an energy barrier of 16.2 kcal/mol again. After the two processes of $\text{C}(\alpha)$ –H deprotonation and $\text{C}(\gamma)$ –protonation, the H on $\text{C}(\alpha)$ is finally transferred to $\text{C}(\gamma)$. Once the *t*-BuO[−] dissociates from **INT18**, reductive elimination comes next to complete the catalytic cycle. Then $\text{C}(sp^2)$ – $\text{C}(sp^2)$ bond was formed through the three-membered ring transition state **TS9** instead of the five-

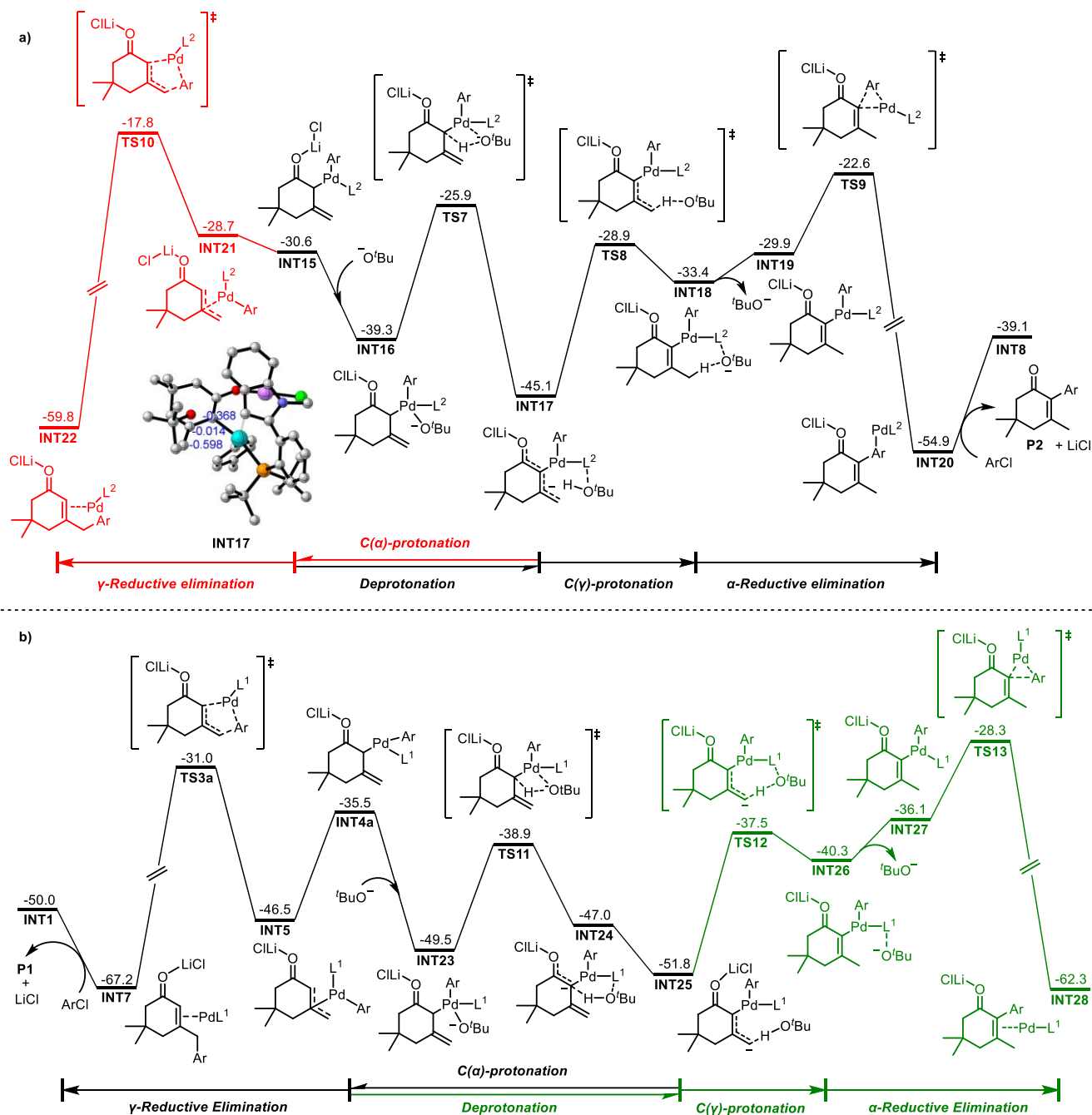


Figure 3. (a) Energy profile for γ -reductive elimination and α -reductive elimination to generate γ - and α -arylated product respectively when the ligand is **L2**. (b) Energy profile for γ -reductive elimination and α -reductive elimination to generate γ - and α -arylated product respectively when the ligand is **L1**.

membered ring transition state because $C(sp^2)$ -Pd cannot isomerize to η^3 -Pd enolate, generating the α -arylated product. In the whole reaction process, the reductive elimination step has the highest activation energy barrier, 22.5 kcal/mol, and the reversible energy barrier is 32.3 kcal/mol, which means that the reductive elimination step is not only the rate-determining step but irreversible.

However, after the formation of intermediate **INT17**, as the energy barrier of the reverse reaction of $C(\alpha)$ -H deprotonation is only 19.2 kcal/mol, **INT17** can return to **INT16** through $C(\alpha)$ -protonation, and then dissociate *t*-BuO⁻ to form **INT15**. Also, because of the η^1 - η^3 - η^1 isomerization, the intermediate **INT15** can isomerize into **INT21** that the isophorone fragment

is bound with the Pd atom in η^3 coordination mode. **INT21** can form γ -arylated products through reductive elimination, and the total energy barrier to γ -arylated products is 27.3 kcal/mol (**TS10**–**INT17**, the three-membered ring reductive elimination process is also unfavorable compared to the five-membered ring, see Figure S6), which is 4.8 kcal/mol higher than the energy barrier of α -arylation route (**TS10** vs. **TS9**), so the α -arylated product will be more favorable kinetically. From the perspective of the entire reaction potential energy surface, however, **INT17** is at the lowest point of the potential energy surface which means **INT17** is the most stable intermediate in the reaction system. Therefore, starting from intermediate **INT17**, both protonation of $C(\gamma)$ or $C(\alpha)$

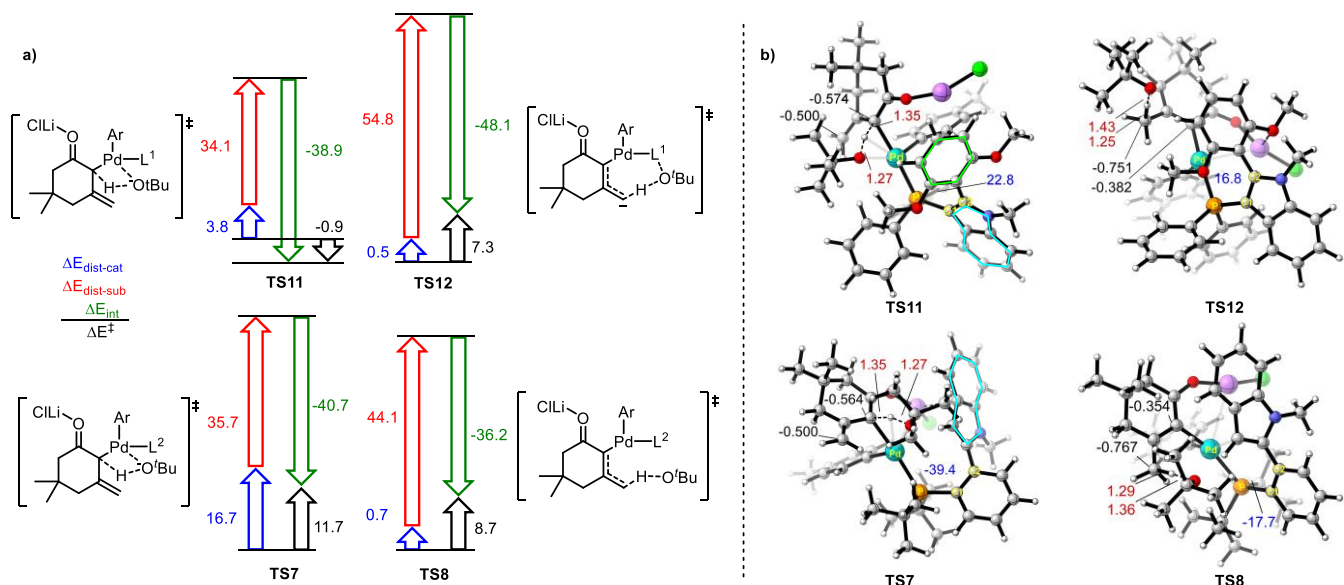


Figure 4. (a) Distortion/interaction analysis for **TS11**, **TS12**, **TS7**, and **TS8**. (b) Corresponding 3D structures for the key transition states, energies are in kcal/mol, and interatomic distances are in Å.

can occur, followed by corresponding reductive elimination to give site-selective products. Thus, for this reaction system, the regioselectivity of the reaction should be determined by the protonation step. The C(γ)-protonation transition state **TS8** has a lower energy barrier than **TS7** by 3.0 kcal/mol when the ligand is **L2**, so C(γ)-protonation has a faster reaction rate than C(α)-protonation and then the α-arylated product is formed after the rate-determining step of reductive elimination.

We also considered the case that the α-arylated product was obtained when the ligand was **L1**. As is shown in Figure 3b, the C(α)-H in **INT4a** can also undergo a deprotonation process through the transition state **TS11** to generate **INT24**. Then the O-H bond in *t*-BuOH swings to the C(γ) position, and the negatively charged C(γ) takes the H back again to generate the C(γ) protonated product **INT26**. Then *t*-BuO⁻ leaves, and **INT27** undergoes reductive elimination to form the α-arylated product. Also, because the process of C(α)-H deprotonation is reversible, **INT25** can return to **INT4a** and then enter the γ-reductive elimination process. It is noteworthy that the energy barrier of C(α)-protonation is 1.4 kcal/mol lower than that of the C(γ) site (**TS11** vs. **TS12**), and the C(α)-protonated product **INT23** has a much lower energy than **INT26** by 9.2 kcal/mol. Therefore, the protonation direction tends to generate **INT23** both kinetically and thermodynamically when the ligand is **L1**. Besides, it is not difficult to find out that the actual total energy barrier of γ-arylation is 21.7 kcal/mol (**TS3a-INT25**) rather than 15.5 kcal/mol mentioned above as **INT25** is the saddle point in the entire PdL¹-catalyzed arylation energy profile.

As the above calculation results show, Pd-catalyzed arylation of unsaturated ketones exhibited different key steps responsible for the observed regioselectivity when two different ligands were utilized. After the deprotonation intermediate was generated, the direction of protonation of the enone fragment determined the following reductive elimination product. To further investigate the effects of ligands on the regioselectivity of the reaction, distortion/interaction analyses^{72, 73} were carried out to the protonation transition states **TS11**, **TS12**, **TS7**, and **TS8**. Each transition state was separated into two

fragments which were palladium enolate complex and *t*-BuOH. The difference in energy between the distorted fragments and optimized ground-state geometries is the distortion energy of palladium enolate complex (ΔE_{dist-cat}) and *t*-BuOH (ΔE_{dist-sub}), respectively. And the difference between the activation energy (ΔE[‡]) and the total distortion energy (ΔE_{dist} = ΔE_{dist-cat} + ΔE_{dist-sub}) is the interaction energy (ΔE_{int}).

As shown in Figure 4a, for **TS11** and **TS12**, the ΔE_{dist-sub} in **TS12** is 20.7 kcal/mol higher while the ΔE_{dist-cat} is 3.3 kcal/mol lower than that in **TS11**, and the ΔE_{int} is 9.2 kcal/mol larger. From the perspective of bond length change, the bond length of O-H is 1.27 Å in **TS11**, while in **TS12** is 1.43 Å, which is elongated 0.16 Å. This greater deviation from the O-H bond accounts for the much higher distortion energy of the *t*-BuOH in **TS12** is likely due to the stronger nucleophilicity of the C(γ), as natural population analysis shows that the charge of C(γ) in **TS12** was found -0.751, while C(α) in **TS11** is only -0.574 (Figure 4b).

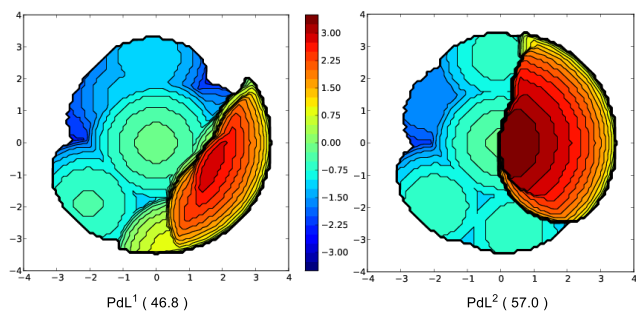


Figure 7. The calculated %V_{Bur} for PdL¹ and PdL² is in parentheses and corresponding steric maps.

When the ligand is **L2**, the corresponding transition states of C(α)-protonation and C(γ)-protonation are **TS7** and **TS8**, respectively. The distortion energy of *t*-BuOH fragment ΔE_{dist-sub} of **TS8** is 8.4 kcal/mol higher, and the catalyst fragment ΔE_{dist-cat} is 16.0 kcal/mol lower than that of **TS7**, and the interaction energy ΔE_{int} is 4.5 kcal/mol smaller than that of **TS7**. Alt-

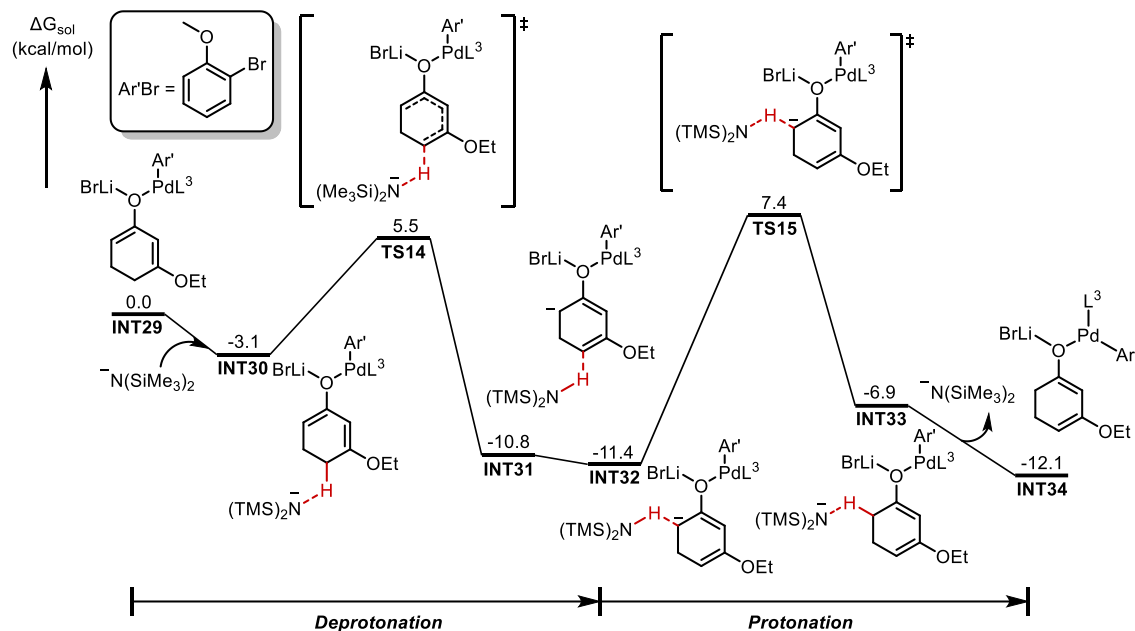


Figure 5. Base-assisted migration mechanism for [1,5]-H migration during γ -arylation of β -alkoxy cyclohexenones.

though the length of the O–H bond in **TS8** is also longer than that in **TS7**, the increase in the $\Delta E_{\text{dist-sub}}$ of **TS8** is not as much as the increase in the $\Delta E_{\text{dist-cat}}$ of **TS7**. Therefore, the reason why the energy of **TS7** is higher than that of **TS8** is mainly that the distortion energy of the catalyst fragment in **TS7** increased too much. From Figure 4b, we can see that the dihedral angle $\angle \text{Pd-P-C1-C2}$ in **TS8** is -17.7° , while in **TS7** it is -39.4° , which increased by 21.7° . For comparison, the dihedral angle of **TS11** changed only 6.0° from that of **TS12**. Therefore, the distortion of the catalyst complex mainly contributed to the increase in the total energy in **TS7**.

Why did the $\Delta E_{\text{dist-cat}}$ increase so much that protonation of the C(α) site was unfavorable when the ligand is **L2**? By carefully inspecting the two transition state structures of **TS11** and **TS7**, we discovered that in **TS11**, the indole ring on the phosphine ligand faces downward, while in **TS7** faces upward. Since tert-butanol is mainly on the top of the phosphine ligand during the C(α)-protonation process, the upper space will be crowded. In **TS11**, as the indole ring faces downward and the benzene ring faces upward whose space volume is smaller than that of the indole ring, the degree of crowding is relieved. Therefore, the distortion of the ligand is slight, and it is also beneficial to C(α)-protonation process. While in **TS7**, this situation is exactly the opposite. To further demonstrate the effect of these two ligands on the steric repulsion, we calculated the buried volume ($\%V_{\text{Bur}}$) and drew the steric maps⁷⁴⁻⁷⁷ around the palladium when the ligands were **L1** and **L2**. As shown in Figure 5, the red areas in the steric maps respectively represent the steric hindrance caused by the aromatic ring in **L1** and the indole ring in **L2**. The steric hindrance caused by the indole ring in **L2** is more significant, so the $\Delta E_{\text{dist-cat}}$ increased by the indole ring will be greater than **TS7**.

The distortion/interaction analysis allows us to conclude that the regioselectivity in the protonation reactions of **INT17** and **INT25** is affected by both the distortion and interaction energies, but the former is the decisive factor in determining which product is formed. Due to the change of steric hindrance brought by different ligands, the protonation process

will proceed in different sites, and finally regioselective arylated products will be obtained.

In 2021, Li-Dong Shao *et al.*²⁵ reported Pd-catalyzed direct γ -C(sp^3)–H arylation of β -alkoxy cyclohexenones, and they found the phenomenon that the H on C(γ) was transferred to the C(α') position during the deuterium labeling experiments. Therefore, they launched a DFT mechanism study on the H migration step, only to find that the energy barrier for direct [1,5]-H shift is so high that it is almost impossible to occur under the experimental conditions (Scheme 1c). Based on our discovery above that the mechanism of [1,3]-H migration is assisted by the base in the reaction system, the base-assisted [1,5]-H migration mechanism for γ -arylation of β -alkoxy cyclohexenones is also calculated, and the results are shown in Figure 5.

Since the main mechanism is similar to the catalytic cycle described above, only the processes that involve [1,5]-H migration are discussed here. Starting from transmetalation product **INT29**, it will first undergo deprotonation of C(γ)–H by the $\text{N}(\text{TMS})_2$ with an activation free energy of 8.6 kcal/mol. Then $\text{HN}(\text{TMS})_2$ moves to the C(α') position, followed by the protonation of the C(α') position. In this way, the direct [1,5]-H shift changed to a deprotonation/protonation process with an activation free energy of 18.8 kcal/mol due to the assistance of $\text{N}(\text{TMS})_2$. In addition, the total energy barrier of this reaction is still 18.8 kcal/mol as the rate-determining step is the C(γ) protonation step from the perspective of the entire potential energy surface (Figure S7 and S8), which is in good agreement with the experimental results that H transfer is involved in the RDS, proving the validity of the proton shuttle model.

CONCLUSIONS

In this study, a detailed mechanism of the Pd-catalyzed regioselective arylation of α,β -unsaturated ketones with aryl halides was comprehensively investigated by DFT calculations. The calculation results reveal that the reactions take place via four sequential processes: oxidative addition of aryl halides to

the Pd(0)L_n; transmetallation between [Pd(II)L_n(Ar)(X)] complex and Li-enolates generated *in situ*; H migration that includes C(α)-H deprotonation followed by C(γ) or C(α) protonation; reductive elimination to form α - or γ -arylated product. The reductive elimination step was found to be the rate-determining step and protonation step was the regioselectivity-determining step. Besides, the Heck-type mechanism for α -arylation of α,β -unsaturated ketones is proved to be infeasible due to the high activation barrier of the insertion step.

In the C(α) or C(γ)-protonation step, the base acts as a proton shuttle to facilitate [1,3]-H migration and determines the regioselectivity of the reaction. By tuning the steric repulsion between the enone fragment and phosphine ligand, C(α)-protonation which is the reverse process of deprotonation can be suppressed and thus turn to C(γ)-protonation followed by a C(sp²)-C(sp²) reductive elimination to generate C(α)-arylated product. Furthermore, the phenomenon of [1,5]-H migration discovered in γ -arylation of β -alkoxy cyclohexenones is also well rationalized by the base-assisted H migration model.

Our results present an in-depth insight into the detailed mechanism of H migration that occurred in the Pd-catalyzed arylation of α,β -unsaturated ketones and reveal the influence of ligands on the regioselectivity, which would be helpful for the optimization of experimental conditions and further development in this area.

ASSOCIATED CONTENT

Supporting Information

The Supporting Information is available free of charge on the ACS Publications website.

Additional computational results and energies of all computed structures (PDF)

Cartesian coordinates of the optimized structures (XYZ)

AUTHOR INFORMATION

Corresponding Author

* **Shuanglin Qu** – College of Chemistry and Chemical Engineering, State Key Laboratory of Chemo/Biosensing and Chemometrics, Hunan University, Changsha 410082, P. R. China; [orcid.org/0000-0002-8122-9848](mailto:squ@hnu.edu.cn); squ@hnu.edu.cn

Author Contributions

Shuanglin Qu supervised and guided the research, and revised the manuscript. Jinbo Luo performed the calculation, summarized the data, and wrote the manuscript. Xiaoxi Su and Zhizheng Chen, helped to summarize the data. All authors contributed to the preparation of the manuscript.

ACKNOWLEDGMENT

We acknowledge financial support from the National Natural Science Foundation of China (No. 21903022) and the Hunan Youth Talent (grant no. 2021RC3053).

REFERENCES

- (1) Davies, H. M.; Du Bois, J.; Yu, J. Q. C-H functionalization in organic synthesis. *Chem. Soc. Rev.* **2011**, *40*, 1855-1856.
- (2) Gutekunst, W. R.; Baran, P. S. C-H functionalization logic in total synthesis. *Chem. Soc. Rev.* **2011**, *40*, 1976-1991.

- (3) Abrams, D. J.; Provencher, P. A.; Sorensen, E. J. Recent applications of C-H functionalization in complex natural product synthesis. *Chem. Soc. Rev.* **2018**, *47*, 8925-8967.
- (4) Johansson, C. C.; Colacot, T. J. Metal-catalyzed alpha-arylation of carbonyl and related molecules: novel trends in C-C bond formation by C-H bond functionalization. *Angew. Chem. Int. Ed.* **2010**, *49*, 676-707.
- (5) Franzoni, I.; Mazet, C. Recent trends in Pd-catalyzed remote functionalization of carbonyl compounds. *Org. Biomol. Chem.* **2014**, *12*, 233-241.
- (6) Wang, M.; Wang, W.; Li, D.; Wang, W. J.; Zhan, R.; Shao, L. D. alpha-C(sp³)-H Arylation of Cyclic Carbonyl Compounds. *Nat. Prod. Bioprospect.* **2021**, *11*, 379-404.
- (7) Palucki, M.; Buchwald, S. L. Palladium-Catalyzed α -Arylation of Ketones. *J. Am. Chem. Soc.* **1997**, *119*, 11108-11109.
- (8) Hamann, B. C.; Hartwig, J. F. Palladium-Catalyzed Direct α -Arylation of Ketones. Rate Acceleration by Sterically Hindered Chelating Ligands and Reductive Elimination from a Transition Metal Enolate Complex. *J. Am. Chem. Soc.* **1997**, *119*, 12382-12383.
- (9) Bellina, F.; Rossi, R. Transition metal-catalyzed direct arylation of substrates with activated sp³-hybridized C-H bonds and some of their synthetic equivalents with aryl halides and pseudohalides. *Chem. Rev.* **2010**, *110*, 1082-1146.
- (10) Pawar, G. G.; Kale, A. P.; Sah, P.; Kapur, M. Total Synthesis of Resorcylic Acid Lactone(-)Neocosmosin A Using Palladium-Catalyzed α -Arylation of Enones as the Key Step. *Eur. J. Org. Chem.* **2022**, *26*, e202201277.
- (11) Jette, C. I.; Geibel, I.; Bachman, S.; Hayashi, M.; Sakurai, S.; Shimizu, H.; Morgan, J. B.; Stoltz, B. M. Palladium-Catalyzed Construction of Quaternary Stereocenters by Enantioselective Arylation of gamma-Lactams with Aryl Chlorides and Bromides. *Angew. Chem. Int. Ed.* **2019**, *58*, 4297-4301.
- (12) Sivanandan, S. T.; Shaji, A.; Ibnusaud, I.; Seechurn, C. C. C. J.; Colacot, T. J. Palladium-Catalyzed α -Arylation Reactions in Total Synthesis. *Eur. J. Org. Chem.* **2015**, *2015*, 38-49.
- (13) Terao, Y.; Satoh, T.; Miura, M.; Nomura, M. Regioselective arylation on the γ -position of α,β -unsaturated carbonyl compounds with aryl bromides by palladium catalysis. *Tetrahedron Lett.* **1998**, *39*, 6203-6206.
- (14) Hyde, A. M.; Buchwald, S. L. Palladium-catalyzed gamma-arylation of beta,gamma-unsaturated ketones: application to a one-pot synthesis of tricyclic indolines. *Angew. Chem. Int. Ed.* **2008**, *47*, 177-180.
- (15) Huang, D. S.; Hartwig, J. F. Palladium-catalyzed gamma-arylation of alpha,beta-unsaturated esters from silyl ketene acetals. *Angew. Chem. Int. Ed.* **2010**, *49*, 5757-5761.
- (16) Franzoni, I.; Guénee, L.; Mazet, C. Access to congested quaternary centers by Pd-catalyzed intermolecular γ -arylation of unactivated α,β -unsaturated aldehydes. *Chem. Sci.* **2013**, *4*, 2619-2624.
- (17) Franzoni, I.; Guénee, L.; Mazet, C. Chiral monodentate phosphine ligands for the enantioselective α - and γ -arylation of aldehydes. *Tetrahedron* **2014**, *70*, 4181-4190.
- (18) Hyde, A. M.; Buchwald, S. L. Synthesis of 5,5-disubstituted butenolides based on a Pd-catalyzed gamma-arylation strategy. *Org. Lett.* **2009**, *11*, 2663-2666.
- (19) Duez, S.; Bernhardt, S.; Heppekausen, J.; Fleming, F. F.; Knochel, P. Pd-catalyzed alpha-arylation of nitriles and esters and gamma-arylation of unsaturated nitriles with TMPZnCl.LiCl. *Org. Lett.* **2011**, *13*, 1690-1693.
- (20) Hao, F.; Nishiwaki, N. Recent Progress in Nitro-Promoted Direct Functionalization of Pyridones and Quinolones. *Molecules* **2020**, *25*, 673.
- (21) Xue, L.; Lin, Z. Theoretical aspects of palladium-catalysed carbon-carbon cross-coupling reactions. *Chem. Soc. Rev.* **2010**, *39*, 1692-1705.
- (22) Franzoni, I.; Poblador-Bahamonde, A. I. Computational study on the mechanism of the palladium-catalyzed arylation of α,β -unsaturated aldehydes. *Organometallics* **2016**, *35*, 2955-2964.

- (23) Orlandi, M.; Licini, G. Computational Analysis of Enantioselective Pd-Catalyzed alpha-Arylation of Ketones. *J. Org. Chem.* **2020**, *85*, 11511-11518.
- (24) Yuen, O. Y.; So, C. M. Ligand Control of Palladium-Catalyzed Site-Selective alpha- and gamma-Arylation of alpha,beta-Unsaturated Ketones with (Hetero)aryl Halides. *Angew. Chem. Int. Ed.* **2020**, *59*, 23438-23444.
- (25) Shao, L.-D.; Chen, Y.; Wang, M.; Xiao, N.; Zhang, Z.-J.; Li, D.; Li, R.-T. Palladium-catalyzed direct γ -C(sp³)-H arylation of β -alkoxy cyclohexenones: reaction scope and mechanistic insights. *Org. Chem. Front.* **2022**, *9*, 2308-2315.
- (26) Ashitha, K. T.; Krishna M. S. A.; D, B.; B. Somappa, S. Recent advances in the transition metal-free synthesis of heterocycles from α,β -unsaturated ketones. *Org. Chem. Front.* **2022**, *9*, 5306-5357.
- (27) Diana, E. J.; Kanchana, U. S.; Mathew, T. V.; Anilkumar, G. Recent developments in the metal catalysed cross-coupling reactions for the synthesis of the enone system of chalcones. *Appl. Organomet. Chem.* **2020**, *34*, e5987.
- (28) Frisch, M. J.; Trucks, G. W.; Schlegel, H. B.; Scuseria, G. E.; Robb, M. A.; Cheeseman, J. R.; Scalmani, G.; Barone, V.; Petersson, G. A.; Nakatsuji, H.; Li, X.; Caricato, M.; Marenich, A. V.; Bloino, J.; Janesko, B. G.; Gomperts, R.; Mennucci, B.; Hratchian, H. P.; Ortiz, J. V.; Izmaylov, A. F.; Sonnenberg, J. L.; Williams, Ding, F.; Lipparini, F.; Egidi, F.; Goings, J.; Peng, B.; Petrone, A.; Henderson, T.; Ranasinghe, D.; Zakrzewski, V. G.; Gao, J.; Rega, N.; Zheng, G.; Liang, W.; Hada, M.; Ehara, M.; Toyota, K.; Fukuda, R.; Hasegawa, J.; Ishida, M.; Nakajima, T.; Honda, Y.; Kitao, O.; Nakai, H.; Vreven, T.; Throssell, K.; Montgomery Jr., J. A.; Peralta, J. E.; Ogliaro, F.; Bearpark, M. J.; Heyd, J. J.; Brothers, E. N.; Kudin, K. N.; Staroverov, V. N.; Keith, T. A.; Kobayashi, R.; Normand, J.; Raghavachari, K.; Rendell, A. P.; Burant, J. C.; Iyengar, S. S.; Tomasi, J.; Cossi, M.; Millam, J. M.; Klene, M.; Adamo, C.; Cammi, R.; Ochterski, J. W.; Martin, R. L.; Morokuma, K.; Farkas, O.; Foresman, J. B.; Fox, D. J. Gaussian 16 Rev. C.01. Wallingford, CT, 2016.
- (29) Lee, C.; Yang, W.; Parr, R. G. Development of the Colle-Salvetti correlation-energy formula into a functional of the electron density. *Phys. Rev. B* **1988**, *37*, 785.
- (30) Becke, A. D. Density-functional thermochemistry. III. The role of exact exchange. *J. Chem. Phys.* **1993**, *98*, 5648-5652.
- (31) Grimme, S.; Antony, J.; Ehrlich, S.; Krieg, H. A consistent and accurate ab initio parametrization of density functional dispersion correction (DFT-D) for the 94 elements H-Pu. *J. Chem. Phys.* **2010**, *132*, 154104.
- (32) Grimme, S.; Ehrlich, S.; Goerigk, L. Effect of the damping function in dispersion corrected density functional theory. *J. Chem. Phys.* **2011**, *32*, 1456-1465.
- (33) Andrae, D. H.; U.; Dolg, M.; Stoll, H.; Preuss, H. Energy-adjusted ab initio pseudopotentials for the second and third row transition elements. *Theoret. Chim. Acta* **1990**, *77*, 123-141.
- (34) Roy, L. E.; Hay, P. J.; Martin, R. L. Revised Basis Sets for the LANL Effective Core Potentials. *J. Chem. Phys.* **2008**, *4*, 1029-1031.
- (35) Hehre, W. J.; Ditchfield, R.; Pople, J. A. Self-Consistent Molecular Orbital Methods. XII. Further Extensions of Gaussian-Type Basis Sets for Use in Molecular Orbital Studies of Organic Molecules. *J. Chem. Phys.* **1972**, *56*, 2257-2261.
- (36) Francl, M. M.; Pietro, W. J.; Hehre, W. J.; Binkley, J. S.; Gordon, M. S.; DeFrees, D. J.; Pople, J. A. Self-consistent molecular orbital methods. XXIII. A polarization-type basis set for second-row elements. *J. Chem. Phys.* **1982**, *77*, 3654-3665.
- (37) Fukui, K. The path of chemical reactions-the IRC approach. *Acc. Chem. Res.* **1981**, *14*, 363-368.
- (38) Zhao, Y.; Truhlar, D. G. The M06 suite of density functionals for main group thermochemistry, thermochemical kinetics, noncovalent interactions, excited states, and transition elements: two new functionals and systematic testing of four M06-class functionals and 12 other functionals. *Theor. Chem. Acc.* **2008**, *120*, 215-241.
- (39) Marenich, A. V.; Cramer, C. J.; Truhlar, D. G. Universal Solvation Model Based on Solute Electron Density and on a Continuum Model of the Solvent Defined by the Bulk Dielectric Constant and Atomic Surface Tensions. *J. Phys. Chem. B* **2009**, *113*, 6378-6396.
- (40) Krishnan, R.; Binkley, J. S.; Seeger, R.; Pople, J. A. Self-consistent molecular orbital methods. XX. A basis set for correlated wave functions. *J. Chem. Phys.* **1980**, *72*, 650-654.
- (41) McLean, A. D.; Chandler, G. S. Contracted Gaussian basis sets for molecular calculations. I. Second row atoms, Z=11-18. *J. Chem. Phys.* **1980**, *72*, 5639-5648.
- (42) Frisch, M. J.; Pople, J. A.; Binkley, J. S. Self-consistent molecular orbital methods 25. Supplementary functions for Gaussian basis sets. *J. Chem. Phys.* **1984**, *80*, 3265-3269.
- (43) Ribeiro, R. F.; Marenich, A. V.; Cramer, C. J.; Truhlar, D. G. Use of solution-phase vibrational frequencies in continuum models for the free energy of solvation. *J. Phys. Chem. B* **2011**, *115*, 14556-14562.
- (44) Wiberg, K. B. Application of the pople-santry-segal CNDO method to the cyclopropylcarbonyl and cyclobutyl cation and to bicyclobutane. *Tetrahedron* **1968**, *24*, 1083-1096.
- (45) Reed, A. E.; Curtiss, L. A.; Weinhold, F. Intermolecular interactions from a natural bond orbital, donor-acceptor viewpoint. *Chem. Rev.* **1988**, *88*, 899-926.
- (46) Weinhold, F. Natural bond orbital analysis: a critical overview of relationships to alternative bonding perspectives. *J. Chem. Phys.* **2012**, *33*, 2363-2379.
- (47) *CYLVIEW20*; Legault, C. Y. Université de Sherbrooke, 2020. <http://www.cylvview.org>.
- (48) Tkachuk, A.; Zagora, A.; Terekhov, I.; Mukhametov, R. Isophorone Diamine-A Curing Agent for Epoxy Resins: Production, Application, Prospects. A Review. *Polym. Sci. Ser. D* **2022**, *15*, 171-176.
- (49) Amatore, C.; Jutand, A.; M'Barki, M. A. Evidence of the formation of zerovalent palladium from Pd(OAc)₂ and triphenylphosphine. *Organometallics* **1992**, *11*, 3009-3013.
- (50) Amatore, C.; Carre, E.; Jutand, A.; M'Barki, M. A. Rates and mechanism of the formation of zerovalent palladium complexes from mixtures of Pd(OAc)₂ and tertiary phosphines and their reactivity in oxidative additions. *Organometallics* **1995**, *14*, 1818-1826.
- (51) Amatore, C.; Jutand, A.; Thuilliez, A. Formation of palladium(0) complexes from Pd(OAc)₂ and a bidentate phosphine ligand (dppp) and their reactivity in oxidative addition. *Organometallics* **2001**, *20*, 3241-3249.
- (52) Li, Z.; Fu, Y.; Guo, Q. X.; Liu, L. Theoretical study on monoligated Pd-catalyzed cross-coupling reactions of aryl chlorides and bromides. *Organometallics* **2008**, *27*, 4043-4049.
- (53) Schoenebeck, F.; Houk, K. N. Ligand-controlled regioselectivity in palladium-catalyzed cross coupling reactions. *J. Am. Chem. Soc.* **2010**, *132*, 2496-2497.
- (54) Sikk, L.; Tammiku-Taul, J.; Burk, P. Computational Study of Copper-Free Sonogashira Cross-Coupling Reaction. *Organometallics* **2011**, *30*, 5656-5664.
- (55) Zeng, G.; Sakaki, S. Noble reaction features of bromoborane in oxidative addition of B-Br sigma-bond to [M(PMe₃)₂] (M=Pt or Pd): theoretical study. *Inorg. Chem.* **2011**, *50*, 5290-5297.
- (56) Casado, A. L.; Espinet, P. Mechanism of the Stille Reaction. 1. The Transmetalation Step. Coupling of R¹I and R²SnBu₃ Catalyzed by *trans*-[PdR¹IL₂] (R¹ = C₆Cl₂F₃; R² = Vinyl, 4-Methoxyphenyl; L = AsPh₃). *J. Am. Chem. Soc.* **1998**, *120*, 8978-8985.
- (57) Melník, M.; Mikuš, P. Stereoisomers of organoplatinum complexes. *J. Organomet. Chem.* **2015**, *799-800*, 239-256.
- (58) Goossen, L. J.; Koley, D.; Hermann, H. L.; Thiel, W. Mechanistic pathways for oxidative addition of aryl halides to palladium(0) complexes: A DFT study. *Organometallics* **2005**, *24*, 2398-2410.
- (59) Braga, A. A. C.; Ujaque, G.; Maseras, F. A DFT study of the full catalytic cycle of the Suzuki-Miyaura cross-coupling on a model system. *Organometallics* **2006**, *25*, 3647-3658.
- (60) González-Pérez, A. B.; Álvarez, R.; Faza, O. N.; de Lera, Á. R.; Aurrecochea, J. M. DFT-Based Insights into Pd-Zn Cooperative Effects in Oxidative Addition and Reductive Elimination Processes Relevant to Negishi Cross-Couplings. *Organometallics* **2012**, *31*, 2053-2058.
- (61) Yang, J. J.; Xu, Z.; Nie, Y. X.; Lu, S. Q.; Zhang, J.; Xu, L. W. Long-Distance Chirality Transfer from P-Ligand to Prochiral

- Dihydrosilanes via Pd(II) Aryl Iodide Complex in Pd-Catalyzed Silylation of Aryl Iodide: A DFT Study. *J. Org. Chem.* **2020**, *85*, 14360-14368.
- (62) Tiekink, E. H.; Vermeeren, P.; Bickelhaupt, F. M.; Hamlin, T. A. How Lewis Acids Catalyze Ene Reactions. *Eur. J. Org. Chem.* **2021**, *2021*, 5275-5283.
- (63) Zhou, B. Y.; Xue, X. S.; Cheng, J. P. Theoretical study of Lewis acid activation models for hypervalent fluoriodane reagent: The generality of "F-coordination" activation model. *Tetrahedron Lett.* **2017**, *58*, 1287-1291.
- (64) Guan, W.; Sakaki, S.; Kurahashi, T.; Matsubara, S. Reasons Two Nonstrained C–C σ -Bonds Can Be Easily Cleaved in Decyanative [4 + 2] Cycloaddition Catalyzed by Nickel(0)/Lewis Acid Systems. Theoretical Insight. *ACS Catal.* **2014**, *5*, 1-10.
- (65) Liu, X. L.; Gu, Z. H. Pd-catalyzed Heck cyclization and in situ hydrocarboxylation or hydromethenylation via a hydrogen borrowing strategy. *Org. Chem. Front.* **2015**, *2*, 778-782.
- (66) Poater, A.; Ragone, F.; Correa, A.; Cavallo, L. Comparison of different ruthenium-alkylidene bonds in the activation step with N-heterocyclic carbene Ru-catalysts for olefins metathesis. *Dalton Trans.* **2011**, *40*, 11066-11069.
- (67) Franzoni, I.; Guénée, L.; Mazet, C. Access to congested quaternary centers by Pd-catalyzed intermolecular γ -arylation of unactivated α,β -unsaturated aldehydes. *Chem. Sci.* **2013**, *4*, 2619-2624.
- (68) Tsutsui, M.; Hancock, M.; Ariyoshi, J.; Levy, M. N. Sigma-Pi Rearrangements of Organotransition Metal Compounds. *Angew. Chem. Int. Ed.* **1969**, *8*, 410-420.
- (69) Yuan, B. F.; He, R. X.; Shen, W.; Li, M. Influence of Base Strength on the Proton-Transfer Reaction by Density Functional Theory. *Eur. J. Org. Chem.* **2017**, *2017*, 3947-3956.
- (70) Qu, S.; Dang, Y.; Wen, M.; Wang, Z. X. Mechanism of the methyltrioxorhenium-catalyzed deoxydehydration of polyols: a new pathway revealed. *Chemistry* **2013**, *19*, 3827-3832.
- (71) Qu, Z. W.; Zhu, H.; Grimme, S. Mechanistic Insights for Aniline-Catalyzed Halogenation Reactions. *ChemCatChem* **2020**, *12*, 5369-5373.
- (72) Bickelhaupt, F. M.; Houk, K. N. Analyzing Reaction Rates with the Distortion/Interaction-Activation Strain Model. *Angew. Chem. Int. Ed.* **2017**, *56*, 10070-10086.
- (73) Green, A. G.; Liu, P.; Merlic, C. A.; Houk, K. N. Distortion/Interaction analysis reveals the origins of selectivities in iridium-catalyzed C-H borylation of substituted arenes and 5-membered heterocycles. *J. Am. Chem. Soc.* **2014**, *136*, 4575-4583.
- (74) Falivene, L.; Cao, Z.; Petta, A.; Serra, L.; Poater, A.; Oliva, R.; Scarano, V.; Cavallo, L. Towards the online computer-aided design of catalytic pockets. *Nat. Chem.* **2019**, *11*, 872-879.
- (75) Poater, A.; Ragone, F.; Giudice, S.; Costabile, C.; Dorta, R.; Nolan, S. P.; Cavallo, L. Thermodynamics of N-heterocyclic carbene dimerization: The balance of sterics and electronics. *Organometallics* **2008**, *27*, 2679-2681.
- (76) Poater, A.; Ragone, F.; Mariz, R.; Dorta, R.; Cavallo, L. Comparing the enantioselective power of steric and electrostatic effects in transition-metal-catalyzed asymmetric synthesis. *Chemistry* **2010**, *16*, 14348-14353.
- (77) Clavier, H.; Nolan, S. P. Percent buried volume for phosphine and N-heterocyclic carbene ligands: steric properties in organometallic chemistry. *Chem. Commun.* **2010**, *46*, 841-861.

Table of Contents

